Submitted to Canadian Metallurgical Quarterly, Jan. 8, 2005.

Mold Slag Property Measurements to Characterize CC Mold – Shell Gap Phenomena

Y. Meng[1], B.G. Thomas[1], A.A. Polycarpou[1], H. Henein[2] and A. Prasad[2]

[1]Dept. of Mechanical & Industrial Engineering, University of Illinois at Urbana-Champaign
[2]Dept. of Chemical & Materials Engineering, University of Alberta, Edmonton, Canada

Abstract

Multi-faceted experiments were conducted to measure the properties of several mold slags, needed for fundamental characterization of heat transfer and friction in the interfacial gap between the shell and mold during the continuous casting of steel. A novel apparatus was used to measure the friction coefficient between solidified mold flux and copper at elevated temperatures. The measured softening temperature is interpreted to extrapolate the slag viscosity-temperature curves far into the low temperature – high viscosity region. Continuous-cooling transformation curves were extracted from XRD analysis of DSC test samples and thermocouple dip tests. Time-temperature transformation curves were obtained from similar analysis of melted mold powder samples that were atomized into droplets, quenched to form glass, and then partially devitrified by reheating to different temperatures for different times and quenched. Polarized light microscopy, SEM, and EDX analysis revealed distinct crystalline and glassy layers, but no severe macro-segregation in a tail-out slag film taken from an operating caster. The results from these new measurements have important implications for the prediction of interfacial gap phenomena, including mold heat transfer, friction, slag layer fracture, and steel surface quality.

I Introduction

In the continuous casting of steel, the choice of mold slag is critically important to the control of heat transfer and lubrication in the mold. Optimal design of the mold slag can produce slow, uniform heat transfer and low friction between the mold and shell. This can avoid surface defects such as longitudinal, transverse and star cracks; enhance surface quality with the formation of uniform and shallow oscillation marks; prevent breakouts; and enable increased casting speed.

Phenomena

Mold powder is added to the top surface above the molten steel, where it sinters and melts into a liquid layer, called mold flux or mold slag, that floats on the molten steel. During mold oscillation, the slag is drawn into the gap between the shell and mold at the meniscus. It cools rapidly against the water-cooled copper mold walls and is partly drawn down by the moving shell, to be consumed during the casting process. The temperature and viscosity gradients across the gap are steep, so the slag forms several different layers.

The consumption rate depends on the temperature-dependent viscosity profile across the liquid layer, and on the layer thickness, which depends greatly on the oscillation mark profile that comprises most of the consumption[1, 2]. The solid layer that freezes against the mold wall at the meniscus includes a rim that greatly affects the complex oscillation phenomena[3]. This layer is initially glassy, if the cooling rate is large enough. Glassy solid layers sometimes crystallize later through a process called “devitrification,” if time in the mold is sufficiently long and the temperature of the solid layer is sufficiently high[4]. The solid layer temperature depends on the mold hotface temperature and the local contact resistance[1]. The thickness of the solid layer gradually increases as crystallization proceeds during the process. The solid layer may fracture

during the oscillation downstroke, if the interfacial friction between the slag and mold is too small, or the strength and fracture toughness of the layer is too low[2]. This causes detrimental nonuniformities in heat transfer[5-7].

Heat transfer in the continuous casting process depends mainly on the thickness, conductivity, and contact resistance of the slag layers in the gap[1, 8]. The effective conductivity drops as the slag crystallizes, owing to the cracks and bubbles that form[9-11]. Contact resistance depends on the surface roughness of the slag layer[12]. The liquid layer provides lubrication between the shell and mold to lower friction-related problems, so long as it is present. This layer may run out part way down the mold, if the steel surface temperature drops below the local slag crystallization temperature.

All these complex phenomena depend greatly on the composition and mineralogy of the mold powder.

Typical mold slag system

The composition and mineralogy of the mold powder greatly affect its behavior, so is varied according to the requirements of different steel grades and casting conditions. The major constituents include CaO, SiO_2, CaF_2, Al_2O_3 and Na_2O. A relevant ternary system for understanding the behavior of many mold slags is the CaO-SiO_2-CaF_2 system, illustrated with the liquidus surface diagram in Figure 1[13]. In a typical mold slag composition range, the ternary compound cuspidine ($3CaO{\cdot}2SiO_2{\cdot}CaF_2$) equilibrates with $CaO{\cdot}SiO_2$, $3CaO{\cdot}2SiO_2$, $2CaO{\cdot}SiO_2$ and CaF_2 in the solid state. Samples containing these compounds melt incongruently. The lines surrounding cuspidine represent isotherms on the liquidus surface, which vary from 1114°C to 1407°C in this region of interest. The asterisks in Figure 1 show the composition of four slags

discussed in this paper, ignoring the other components. The reported solidus temperature of cuspidine is about 1100°C[14]. The actual phases in the mold slag film are even more complicated because all these components may react together to form new phases and change the eutectic point in addition to being affected by about ten other minor constitutes.

Slag Property Measurement

The complex behaviors of mold slags are difficult to characterize because they depend on many different material properties, including thermal, fluid, and mechanical properties. The melting rate, viscosity, solidification temperature, crystallinity, conductivity, and radiation absorption are typical properties measured to characterize slags in previous work[10, 15-20]. However, the melting rate is a semi-empirical property that combines together several different material properties, including the latent heat and thermal diffusivity, and also depends greatly on process conditions. The other properties vary greatly with time and temperature history, and have not been measured over the entire temperature range of interest. Finally, many of the important properties, such as friction coefficient, strength, and toughness, have almost never been measured.

In-situ "friction signals" can be obtained by installing lubrication sensors[21], load cells[22] or pressure sensors[23] onto the operating continuous casting mold to record the mold speed, and load or pressure variation during mold oscillation. However, fundamental understanding of the meaning of these measurements and how to interpret them to solve problems is lacking. Currently mold friction measurements are evaluated mainly as a means to detect problems with the oscillation system, such as mold misalignment. With better understanding of friction behavior, then friction monitoring could be used to identify the status of mold lubrication to predict surface defects[21] and to help prevent breakouts[24].

Viscosity of the mold slag is highly temperature dependent. In previous work, the viscosity is often expressed as an Arrhenius-type relationship including the effect of composition [25-27]. These models provide a method to design the slag composition to achieve a desired viscosity curve. However, none of them can accurately predict the viscosity near the solidification temperature. These models are only good for the low viscosity, high temperature range ($<10^3$poise) and cannot accommodate the sharp viscosity increase that occurs at lower temperatures. Due to the difficulty of measuring high viscosity, slag viscosity measurements are seldom reported greater than 10Pa·s (100poise). Thus, the viscosity-temperature curve near the solidifying temperature is yet unclear for the mold slags used in continuous casting.

Recent laboratory experiments show that heat transfer across the gap is significantly affected by the crystallization of the slag film while it is relatively insensitive to composition [15]. Several different experimental methods have been used to observe and measure the fraction of crystalline phase formed in slags for different thermal conditions and atmospheres. These include in-situ methods such as single or double hot thermocouple techniques (SHTT/DHTT)[28, 29], and Confocal Microscopy[30], and instrumented cooling methods, such as differential thermal analysis (DTA)[31, 32], quenching[33], step chill molds, and mold simulators[9] followed by microscopic analysis. Isothermal transformation (TTT) diagrams and continuous cooling transformation (CCT) diagrams have been constructed from controlled laboratory experiments [17, 28, 30, 32, 34]. However, most of these methods are limited to relatively low cooling rates (1^oC/min~900^oC/min). The average cooling rate of the mold slag in the longitudinal (meniscus to mold exit) and transverse (mold hot face to steel shell surface) directions may be about 20~25^oC/sec, and the local cooling rate may be as high as 50~100^oC/sec, especially near the meniscus where the maximum heat flux enters the mold. Thus, a method to achieve higher cooling rate would help in studying mold slag

crystallization [35]. In this work, several experiments were performed to measure new slag properties, including the friction coefficient between the slag and mold wall, the viscosity at low temperature, the glassy or crystal structure of the solidified flux, CCT and TTT curves, and the crystalline phases.

II Experimental

A Materials

In this study, four different mold powders were investigated. These are S1 and K1 crystalline slags, S2 glassy slag, and H1 mixed slag-layer film sample taken during tail-out from an operating caster. Their compositions are listed in Table I, which have been re-calculated from the original suppliers report (Table II) by converting F to CaF_2. It must be noted that the carbon is added to slow down the mold powder melting rate and thereby control melting uniformity during the casting process. This carbon burns out during the powder sintering and melting process, so it is not generally present in the liquid slag layer or in the re-solidified slag film in the gap. Thus, the powder for slag samples S1 and S2 were prepared without adding the carbon in order to reproduce the actual molten slag entering the meniscus region in the continuous casting mold, without having to experience the experimental difficulties associating with decarburization.

B Friction Coefficient Tests

Previous modeling work[1, 2] has shown that the slag properties near the solidification temperature are very important to interfacial lubrication. However, previous measurements focused only on the slag properties at high temperature (greater than 1000°C)[27, 36-40]. The lubrication properties of the flux near the softening temperature are rarely reported. Thus, laboratory experiments were

conducted to measure the friction coefficient between the solid slag layer and the mold or steel shell, from room temperature up to 1000°C.

Samples of powders S1 and S2 were melted in a graphite crucible at 1400°C for an hour, and then poured into a preheated metal sample holder and allowed to air cool. Each sample holder was 20-30mm inner diameter and 5mm in depth. The polished sample was then tested in a High Temperature Tribometer (HTT). The HTT is a pin-on-disc apparatus which can measure detailed friction and wear data on test specimens up to 1000°C[41]. A photograph of the apparatus is depicted in Figure 2(a), and Figure 2(b) shows a schematic of the contact configuration. The HTT consists of a rotating/oscillating lower spindle on which the plate specimen is rigidly mounted and a special top holder which applies a 10N contact load through a pin from the top, while in-situ measuring both the normal and friction forces. At the end of the stationary top sample holder there is a 0.25inch diameter steel ball acting as the pin that is positioned off-center against the rotating disk sample (see Figure 2(b)). Figure 2(c) shows the pictures of slag samples before tests. The wear track diameter was set to 0.375inch. The spindle velocity was continuous and varied from 50rpm to 300rpm, resulting in linear velocities of 0.05m/s and 0.3m/s, respectively. Both the (pressure) and transverse (shear) forces are recorded in order to compute the friction coefficient. Temperature was controlled in the air atmosphere inside the bell-jar heating furnace by adjusting power through the 2kW radiation Inconel heating coils in the outer walls, with feedback from a single thermocouple.

The first series of experiments were conducted starting at room temperature, and increasing in 100°C intervals until the machine limit of ~1000°C. It took 3~5 minutes for temperature to reach each of the ~10 different set points. After waiting 5 minutes, data was recorded from the display every two seconds for two minutes, giving 60 data points for each set. To investigate

reproducibility and the importance of heating or cooling history in the apparatus, the second series of experiments was conducted by heating to the highest temperature in only 40 minutes and recording data during decreasing temperature intervals using the same recording procedure. Wear track depths were measured with a profilometer which can quantify depth from 0.02mm to 25mm[42].

C Time-Temperature Transformation Tests

The onset of crystallization is a strong function of cooling history in slags. Three methods were used to investigate continuous cooling transformation phenomena in slags S1 and S2 over a wide range of cooling rates. A fourth method was used to investigate devitrification during furnace holding after the reheating of previously-quenched samples.

DSC Tests Slags S1 and S2 were analyzed by coupling Thermal Gravimetry / Differential Scanning Calorimetry (TG/DSC) tests. Decarbonized mold powder was poured into a ~1g platinum micro-crucible. Pure alumina (Al_2O_3) was selected as the reference for all tests conducted. The temperature was increased from room temperature to 1300°C for slag S1 and 1100°C for slag S2 at a heating rate of 10°C/min. These temperatures were sufficient to fully melt each powder. Each sample was then cooled to room temperature at cooling rates of 1°C/min, 5°C/min and 30°C/min in separate tests. The onset temperature of each exothermic peak indicates a crystallization reaction.

Dip Thermocouples To investigate intermediate cooling rates, a series of thermocouple dip tests were conducted. In these tests, a K-Type Thermocouple with positive Chromel wires and negative Alumel wires, with a bare ~1-mm diameter bead, is dipped into the slag melt in a graphite crucible. It takes a few seconds for the thermocouple to heat up to the slag temperature and reach thermal equilibrium. Then the thermocouple is withdrawn into the air, with a droplet

of the slag stuck around the thermocouple bead. The temperature of the thermocouple is continuously recorded by the data acquisition system. By adjusting the initial melt temperature, or by exposing the dip around the thermocouple to different atmospheric conditions, such as forced convection, a range of cooling rates, 0.5°C/sec~50°C/sec, could be achieved. Sudden drops in cooling rate often correspond to crystallization reactions. Final microstructures were analyzed for crystallization and composition.

Atomization (Glass Formation) The real continuous casting process involves rapid initial quenching of the liquid slag against the mold wall followed by slower cooling at different rates according to position in the slag layer. To reproduce the high cooling rates, an Impulse Atomization Process (IAP) was used. The IAP is a single fluid atomization technique capable of producing droplets of a predictable mean particle size with a relatively tight standard deviation under controlled atmospheric conditions[35]. The mold powder was placed in a graphite crucible and heated to melting in an enclosed tower in a nitrogen atmosphere. At the bottom of the crucible, an array of orifices was machined. By vibrating a plunger inserted into the melt, the molten slag is forced out of the orifices at the bottom of the crucible. The streams disintegrate into droplets according to the vibration frequency and fall through the chamber. The cooling history of the droplets was then predicted using a simple mathematical model of lumped droplet solidification [43]. By varying the atomization parameters to change the radiation and convection conditions, particle cooling rates were obtained ranging from 100°C/sec to 13000°C/sec depending on particle size. After the experiments, a thin film of black deposit was observed on the furnace walls, indicating selective volatilization of a small amount of some mold powder compound(s), likely CaF_2. Figure 3 shows a schematic of the Impulse Atomization Process[35].

Devitrification Tests (Furnace Holding) The atomized slag droplets were confirmed to be in a fully glassy state through XRD measurements. This amorphous material was then subjected to reheating and furnace holding to investigate devitrification. The particles were put into a preheated furnace maintained at different temperatures (500°C to 1100°C), held for a set time (1minute to 2hours), taken out, water quenched to room temperature, and analyzed.

D Sample Analysis

In order to investigate the evolution of crystallization, all of the slag powder and re-solidified slag samples from continuous cooling and devitrification tests were submitted for X-Ray diffraction (XRD) analysis with Cu K_α radiation to examine the phases present. A piece of film of slag H1 from interfacial steel shell/mold gap was caught as it folded off the mold wall during tail-out after a continuous casting sequence. The slag film was cut into thin slices only 0.03mm thick and mounted on microscope slides. The thin section specimen was then observed under polarized light microscopy in order to distinguish its glassy / crystalline structure. To further investigate the morphology and composition distribution of the slag film, an SEM microstructure analysis was carried out with an energy dispersive x-ray spectroscopy system (EDX).

III Results and Discussion

A Friction Coefficient

Figure 4(a) shows a sample of data recorded by the HTT for slag S1 in run #5 at 400°C. Both the average and the variations change with conditions. Figure 4(b) plots the average friction coefficient for 25mm/s rotation velocity, with the variation range shown as min-max "error" bars, indicating the full range of data measured at each test temperature. The average drops slightly,

while the variations generally increase at higher temperatures. Increasing the rotation velocity causes the friction coefficient to increase slightly, but this effect is negligible for temperatures above 500°C, as shown in Figure 4(c). The same behaviors were observed for slag S2.

Figure 5(a) summarizes the results of three friction tests using slag S1. The direction of the arrow on each line shows the evolution of temperature during heating or cooling. The friction coefficient varies between runs with an average value of 0.16 ± 0.1. Increasing temperature above 800°C causes the friction coefficient to begin to drop. This decrease is likely caused by softening of the slag, but might alternatively correspond to formation of an oxidation layer on the top steel ball bearing pin. In general, there is a slight trend of decreasing average friction coefficient with increasing temperature, which is consistent with a softening phenomenon. However, the large variations can be explained by oxidation. An oxide layer is believed to lubricate the metal/slag interface[44]. This would explain the hysteresis loop in run #7, as the lower friction at later times at the same temperature, likely corresponds with oxide layer build-up. The increase of friction just after reversing to decrease temperature at the beginning of runs #5 and #8 might be due to spalling off of the oxide.

Figure 5(b) shows the friction coefficient as a function of temperature for slag S2. It appears that the friction has a slight drop from room temperature to 500°C. Just above 500°C, however, the friction coefficient increases sharply from 0.1 to 0.5. This is because the specimen begins to soften greatly. Instead of wear, the steel ball pin plows through the tacky slag layer and causes an artificially high increase of friction coefficient. Figure 6 shows pictures of the specimens after the friction tests. It confirms that the sample slag S2 became soft and deformed greatly during Run #6, while slag S1 showed only abrasive friction/wear after Run #5. With increasing temperature, the S2 specimen became too soft to withstand any normal force. After this

softening and accompanying deformation, decreasing temperature caused the friction coefficient to fluctuate greatly. This indicates that the surface shape was too rugged to make any effective measurement, which also happened to a specimen where open bubble holes appeared in the wear track. For the test with slag K1, a similar friction increase with material softening was observed at 720^{o}C. The more gradual increase for this test might be due to the use of a different top pin with a flat surface.

The results show that the friction is relatively insensitive to the microstructure of the slag. It generally stays below 0.2 before softening. The softening of the mold slag, indicated by the apparent dramatic increase in friction coefficient, occurs at much lower temperature than previously supposed. This work for the first time enables extension of the slag viscosity curves to a lower temperature range.

B Viscosity

Viscosity and solidification temperature have been identified as the key physical properties in selecting a mold powder with suitable heat transfer properties. Together with the chemical composition, powder manufacturers commonly measure viscosity at high temperature, as shown in Figure 7. Usually only the low-viscosity part of the curve (<400poise) is measured with a viscometer. Higher viscosities cause the viscometer spindle to slip or even break, so cannot be measured.

The high temperature friction test results show that slags S2 and K1 soften at 500^{o}C and about 720^{o}C, and that slag S1 likely begins to soften at 1000^{o}C or above. For slag S2, the normal force dropped from 10N to 7N in about one minute while the donut-shaped wear track depression grew to 0.5mm deep. The magnitude of the slag viscosity at the softening point can be estimated roughly from these results using its definition assuming Newtonian flow:

$$\mu = \frac{\tau_{\theta z}}{\dot{\gamma}_{\theta z}} \tag{1}$$

The shear stress, $\tau_{\theta z}$ can be estimated from the recorded friction force, *F*, and the contact area, *A*:

$$\tau_{\theta z} = \frac{F}{A} \approx \frac{F}{\pi r h} \approx \frac{3.0N}{3.14 \times 3.175mm \times 0.01mm} \approx 30 \times 10^6 Pa \tag{2}$$

Where, *r* is the radius of the spherical pin, *h* is the increase in depression depth over one revolution. The strain rate, $\dot{\gamma}_{\theta z}$ can be estimated by assuming $\frac{\partial v_z}{\partial \theta} = 0$:

$$\dot{\gamma}_{\theta z} = \frac{\partial v_\theta}{\partial z} + \frac{1}{r}\frac{\partial v_z}{\partial \theta} = \frac{\partial v_\theta}{\partial z} \approx \frac{\Delta v_\theta}{\Delta z} \approx \frac{25mm/\sec}{5mm} = 5\sec^{-1} \tag{3}$$

Where, Δz is the slag sample thickness, and v_θ is the linear speed of rotation. Combining equations (1)-(3) gives a viscosity of about $6 \times 10^7 Poise$. This value matches with the viscosity of common glass at its softening point[45]. Thus, another point can be added to the viscosity curves. Figure 7 shows estimates of the entire viscosity curves interpolated down to the low-temperature high- viscosity (10^8poise) region; the high-temperature low-viscosity (<1000Poise) measured data were supplied by the powder manufacturers. It is interesting to note that inflection(s) occur in the high temperature portion of each curve, perhaps due to partial crystallization.

C Phase Characterization

XRD analysis was carried out for the initial decarbonized slag powder, re-solidified atomization particles and samples after the thermocouple dip tests and furnace holding tests. Figure 8 displays the intensity distribution as a function of diffraction angle for the slag powders before melting, and indicates that the six main phases are: silica (SiO_2), calcium fluoride (CaF_2),

wollastonite ($CaSiO_3$), calcite ($CaCO_3$), calcium silicate (Ca_3SiO_5) and sodium carbonate (Na_2CO_3).

The crystalline phases identified in the furnace holding devitrification tests are summarized in Table III and Table IV. The atomized particles had no peaks for crystalline phases, indicating that all droplets of both slags were completely amorphous. The peaks are weaker relative to the background noise for all samples, compared with the slag powder, which indicates that the melting and re-solidification produced some glass in every test. Cuspidine ($3CaO•2SiO_2•CaF_2$) is identified in all non-amorphous specimens. The thermocouple dip tests for slag S1 with slower cooling rates indicate calcium silicon oxide fluoride ($SiO_2•2CaF_2$) phase also. These results show that cuspidine crystallizes easily and that $SiO_2•2CaF_2$ crystallizes at higher temperatures and can be suppressed by higher cooling rates.

In slag S1, the first (easiest) phase to form is cuspidine which first appears after holding at 700°C for 30 minutes. With increasing furnace temperature, different phases are found, as shown in Figure 9. Calcium silicon oxide fluoride ($SiO_2•2CaF_2$) and nepheline ($Na_2O•Al_2O_3•2SiO_2$) are found at temperatures greater than 900°C. Holding slag S1 longer than one hour at 1100°C causes the peaks of nepheline to disappear and a new phase, gehlenite ($2CaO•2Al_2O_3•SiO_2$) to form, as shown in Figure 9(a). This phenomenon was also observed by Grieveson[46] and O'Malley[47].

For slag S2, no crystalline phase forms at 500°C even after two hours of holding. Besides the common cuspidine phase, some new phases such as nepheline and calcium silicate ($2CaO•SiO_2$, $8CaO•5SiO_2$) can form when holding at 700°C for two hours, or at higher temperatures. Instead of the gehlenite found in slag S1, a sodium calcium silicate phase ($Na_2O•2CaO•3SiO_2$) is found in slag S2 at 900°C. When the holding temperature is near to the slag melting temperature, only

a small amount of crystalline cuspidine is observed in the amorphous background (Figure 9(b)). This might due to the lower driving force for crystallization at higher temperature.

D CCT Curves

Figure 10 shows typical DSC curves for slags S1 and S2 generated at a constant heating rate of 10°C/min and cooling rate of 1°C/min. The sharp endothermic trough of the heating curves at 100°C is due to water evaporation. Endothermic troughs are also found at ~450°C and 750°C in Slag S1 and ~700-750°C for Slag S2. These troughs are most likely associated with the decomposition of the two common carbonates found in these mold fluxes: Na_2CO_3 at 450°C and $CaCO_3$ at 750°C [16]. This is confirmed by the accompanying weight loss included in Figure 10(a) (TG), which is expected because of the volatilization of CO_2. The series of endothermic peaks above 1000°C on the heating curve indicates that the powder began to melt incongruently, as the different minerals reach their independent liquidus temperatures. The end of the last peak encountered on heating presumably represents the highest liquidus temperature. This is seen to be 1235°C for slag S1 and 1050°C for slag S2.

During the cooling process, the phase transformations are very different from heating, owing to the irreversible chemical reactions that occur during melting. Several exothermic peaks are observed, which again indicate phase transformations. Each phase transformation is believed to begin at the inflection point starting each peak during cooling. For slag S1 cooling at 1°C/min , the exothermic peaks begin at 1234°C, 1160°C and 1022°C, which likely correspond to the onset of three different crystalline phases forming. In general, a higher cooling rate increases the peak height, whereas a lower rate yields higher resolution[14]. Higher cooling rates delay both the onset and finish of each phase transformation.

The cooling curves recorded during the thermocouple dip tests were smoothed using the Savitzky-Golay polynomial smoothing filter to eliminate noise. The filter coefficients: the order of the polynomial, *K*, the number of passes, *P* and the frame size, *F* are taken to be 2, 3, 9. These values are chosen to preserve higher moments in the data, thus reducing the distortion of essential features of the data such as peak heights and line widths in the spectrum, while efficiently suppressing random noise that degrades derivative calculation. Figure 11(a) compares the recorded thermocouple temperature and the filtered curve.

The temperature history curves were numerically differentiated with second order accuracy to distinguish points where the thermal gradient changes would indicate crystallization[48]. As an example, Figure 11(b) shows two points marking the onset of sharp drops in cooling rate where the beginning of crystallization is believed to occur for slag S1 test K. Similar analyses were conducted for other recorded thermocouple data curves. These points were used to construct continuous cooling transformation (CCT) curves.

From the time-temperature profiles recorded during the DSC tests and thermocouple dip tests, CCT diagrams were constructed, taking the time to start at zero when the cooling curves cross the liquidus temperature (1235^{o}C for slag S1 and 1050^{o}C for slag S2). The CCT diagrams are shown in Figure 12(a) and (b) for slag S1 and S2 respectively. The critical cooling rate to maintain the amorphous structure is estimated to be 50^{o}C/s for slag S1, and only 20^{o}C/s for slag S2, which confirms its more glassy nature. These values are similar to critical cooling rates reported elsewhere[29, 32, 49].

At slower cooling rates, below ~1^{o}C/s, relatively equilibrium transformation occurs. The first crystalline phase appears at around the liquidus temperature, which should be cuspidine according to the XRD analysis. Watanabe measured that the liquidus of cuspidine varies between

1114°C (55% CaF_2) and 1407°C (20% CaF_2) in the CaO-SiO_2-CaF_2 ternary system[13]. For slag S1, the liquidus temperature should be ~1250°C, which almost exactly matches the present work. The 1050°C liquidus temperature of slag S2 is found to be lower. This might be due to the effect of the many other compounds in the slag, especially Na_2O, Al_2O_3 etc, which decrease the system melting temperature.

When the cooling rate is slower than ~10°C/s a second crystalline phase forms at around 1100°C in slag S1. This could be calcium silicon oxide (oxy) fluoride (SiO_2 $2CaF_2$) phase. The DSC tests with very slow cooling rate (<5°C/min) shows a third peak near 900°C as shown in Figure 10(a). This implies the existence of a third phase (possibly nepheline) which could not be distinguished in the XRD pattern of the thermocouple dip tests. The cooling curves of the dip tests are more ambiguous but do not appear to show the third phase either. This suggests that this phase is suppressed at the faster cooling rate of the dip tests relative to the DSC tests.

The XRD results from furnace heating devitrification tests confirm that more crystalline phases form at 900°C to 1100°C. Comparing these results with the phase diagrams[13], these phases generally show lower –temperature liquidus lines which is due to the eutectic reaction. The other crystalline phases observed in the isothermal aging tests for slag S2 are difficult to distinguish unambiguously in the XRD pattern and cooling curves of thermocouple dip tests.

E Slag Film Microstructure

A piece of slag K1 film sample was taken from an experimental apparatus, which was constructed to simulate the gap in the real caster[9]. The sample was observed under SEM and Figure 13 show the backscatter electron (BSE) images. This figure reveals a complex multiple-layered structure that is similar in appearance to slag samples, such as slag film H1, that have

been removed from the operating continuous casting mold. The layers in film K1 appear mainly crystalline, and correspond to different cooling rates. On the mold side, the fine and close dendrite structure is consistent with the fast cooling experienced there. In the middle of the film, the grains are uniform with a larger size. The steel side shows uneven-sized grains, which indicates that there was significant growth of a few grains formed during slow cooling, within a glassy background that was likely formed during fast air cooling after the sample was removed.

Figure 14(a) shows the different layers and cracks in the slag film H1 under plane polarized light. Figure 14(b) contains the images under cross polarized light. The extinction on the layer on the molten-steel side proves that it is isotropic. Because crystals of any size or composition have some anisotropic properties, this indicates that the layer closest to the steel is a glassy layer. This suggests that the layer was formed from air quenching the liquid slag while obtaining the sample. Note that the critical cooling rate for obtaining glass is well below typical cooling rates encountered during air cooling, so this finding is reasonable.

Figure 15(a) shows the backscatter electron (BSE) image of the slag H1 film. Figure 15(b) is a close-up of the interface between the two layers. Crystals on the left can be clearly seen growing into the glassy layer on the right. This is consistent with the direction of growth expected after air quenching the right side. This figure clearly reveals the individual crystals of different compounds that grow together from this complex ceramic melt.

To investigate the composition distribution in the specimen, a series of EDX mappings was performed. Each image was created by mapping the X-ray intensity at each point for a specific element. The results, shown in Figure 16, use increasing brightness to indicate where the specific element has higher concentration. On the right hand side (steel side) of each image, all elements are distributed homogenously, which again confirms the glassy microstructure of the steel side.

The EDX spectrum was also used to identify the element composition of different regions in the sample. The left crystalline side (mold side) is composed mainly of high-calcium grains in a high-silicon background. These grains likely represent crystals of cuspidine that precipitated first, followed by crystallization of other compounds, and finally leaving a portion of the remaining background as glassy. The results also indicated that the area average composition is almost the same for the crystal and glassy regions, and at different places in each region. This important finding indicates that no severe macro-segregation occurred in the gap during casting.

IV Summary

Experiments were conducted to measure some important but rarely-measured properties of mold slags used in the continuous casting of steel. These properties include friction coefficient, viscosity at low temperature, CCT curves, TTT curves, and crystal structure composition.

1. Tribometer pin-on-disk measurements show that below the glass transition temperature, the friction coefficient is $\sim 0.16 \pm 0.1$ and increases slightly with increasing temperature.

2. A dramatic rise in apparent friction indicates when the slag begins to soften, which occurs at temperatures as low as 500°C. This softening point allows the slag viscosity – temperature curve to be extended up to 10^8 poise range.

3. XRD analysis of the mold powders and the samples from DSC tests, and thermocouple dip tests all show that Flourine exists as CaF_2 in pre-melted mold powder and cuspidine ($3CaO \cdot 2SiO_2 \cdot CaF_2$) is the predominant phase crystallizing in re-solidified slag.

4. The critical cooling rates for 100% glass are 50°C/sec for crystalline slag S1 and 20°C/sec for glassy slag S2.

5. CCT curves are constructed for two different slags, based on DSC tests, thermocouple dip tests, and isothermal devitrification tests. The latter transformation data were obtained from XRD analysis of melted mold powder samples that were atomized into droplets, quenched to form glass, partially devitrified by reheating to different temperatures for different times, and water quenched.

6. The slag crystallization temperatures and products depend greatly on cooling rate. Cuspidine is the easiest crystalline phase to form in both slags. Slag S1 also crystallizes calcium silicon oxide fluoride (SiO_2•$2CaF_2$), nepheline (Na_2O•Al_2O_3•$2SiO_2$), and gehlenite ($2CaO$•$2Al_2O_3$•SiO_2). The nepheline only forms at higher temperatures and appears to decompose into gehlenite for a longer holding time at high temperature. Slag S2 also crystallizes calcium silicate ($2CaO$•SiO_2, $8CaO$•$5SiO_2$) and sodium calcium silicate (Na_2O•$2CaO$•$3SiO_2$).

7. Polarized light microscopy, SEM and EDX images show crystalline and glassy layers but no severe macro-segregation in the tail-out slag film taken from an operating caster.

More measurements such as reported here are needed to characterize mold slag behavior, heat transfer and friction in the interfacial gap between the shell and mold during the continuous casting of steel.

Acknowledgements

The authors would like to thank the Continuous Casting Consortium of the University of Illinois and the National Science Foundation (Grant DMI-01-15486) for financial support. Some analyses were carried out in the Center for Microanalysis of Materials, University of Illinois, which is partially supported by the U.S. Department of Energy under grant DEFG02-91-ER45439. The support of the National Sciences and Engineering Research Council of Canada is

also gratefully acknowledged. Thanks are also extended to Tim Solzak, Xiaoqiang Hou and Fang Huang for help with the experiments and to Craig Lundstrom and David Payne for suggestions.

References

1. Y. Meng and B.G. Thomas: "Heat Transfer and Solidification Model of Continuous Slab Casting: CON1D", *Metall. Mater. Trans. B (USA),* 2003, vol. 34B (5), pp. 685-705.

2. Y. Meng and B.G. Thomas: "Modeling Transient Slag Layer Phenomena in the Shell/Mold Gap in Continuous Casting of Steel", *Metall. Mater. Trans. B (USA),* 2003, vol. 34B (5), pp. 707-25.

3. E. Takeuchi and J.K. Brimacombe: "The Formation of Oscillation Marks in the Continuous Casting of Steel Slabs", *Metall. Trans. B,* 1984, vol. 15B (3), pp. 493-509.

4. R.J. O'Malley and J. Neal: "An Examination of Mold Flux Film Structures and Mold Gap Behavior Using Mold Thermal Monitoring and Petrographic Analysis at Armco's Mansfield Operations", *Proc. METEC Congress 99*, (Dusseldorf, Germany, 13-15 June, 1999), Verein Deutscher Eisenhuttenleute, Dusseldorf, Germany, 1999, vol.

5. Y. Nakamori, Y. Fujikake and K. Tokiwa: "Development of Friction Measuring System in a Continuous Casting Mold", *Tetsu-to-Hagane (J. Iron Steel Inst. Jpn.),* 1984, vol. 70 (9), pp. 1262-68.

6. J.A. DiLellio and G.W. Young: "Asymptotic model of the mold region in a continuous steel caster", *Metallurgical and Materials Transactions B: Process Metallurgy and Materials Processing Science,* 1995, vol. 26B (6), pp. 1225-441.

7. M.M. Wolf: "Review of Mould Fricrtion", *BHM,* 2000, vol. 145 (7), pp. 270-75.

8. R.B. Mahapatra, J.K. Brimacombe and I.V. Samarasekera: "Mold Behavior and Its Influence on Quality in the Continuous Casting of Steel Slabs. II. Mold Heat Transfer, Mold Flux Behavior, Formation of Oscillation Marks, Longitudinal Off-Corner Depressions, and Subsurface Cracks", *Metall. Trans. B,* 1991, vol. 22B (6), pp. 875-88.

9. D.T. Stone and B.G. Thomas: "Measurement and modeling of heat transfer across interfacial mold flux layers", *Canadian Metallurgical Quarterly (Netherlands),* 1999, vol. 38 (5), pp. 363-75.

10. V. Vermeulen, E. Divry and M. RIgaud: "The Influence of Chemical Composition on the Crystallization and the Heat Transfer of Synthetic Mould Fluxes", *Canadian Metallurgical Quarterly,* 2004, vol. 43 (4), pp. 527-34.

11. K.C. Mills, S. Sridhar, A.S. Normanton and S.T. Mallaband: "Mould flux behaviour in continuous casting", *The Brimacombe Memorial Symposium*, (Vancouver, British Columbia, Canada, 1-4 Oct. 2000), Canadian Institute of Mining, Metallurgy and Petroleum, Montreal, PQ, Canada, 2000, vol., pp. 781-94.

12. K. Tsutsumi, T. Nagasaka and M. Hino: "Surface roughness of solidified mold flux in continuous casting process", *ISIJ Int. (Japan),* 1999, vol. 39 (11), pp. 1150-59.

13. T. Watanabe, H. Fukuyama and K. Nagata: "Stability of cuspidine (3CaO2SiO sub 2 CaF sub 2) and phase relations in the CaOSiO sub 2 CaF sub 2 system", *ISIJ International (Japan),* 2002, vol. 42 (5), pp. 489-97.

14. T. Watanabe, H. Fukuyama, M. Susa and K. Nagata: "Phase diagram cuspidine (3CaO2SiO sub 2 CaF sub 2)-CaF sub 2", *Metallurgical and Materials Transactions B (USA),* 2000, vol. 31B (6), pp. 1273-81B.

15. R. Taylor and K.C. Mills: "Physical Properties of Casting Powders III: Thermal Conductivities of Casting Powders", *Ironmaking and Steelmaking (UK),* 1988, vol. 15 (4), pp. 187-94.

16. K.C. Mills, A. Olusanya, R. Brooks, R. Morrell and S. Bagha: "Physical Properties of Casting Powders. IV. Physical Properties Relevant to Fluid and Thermal Flow", *Ironmaking and Steelmaking,* 1988, vol. 15 (5), pp. 257-64.

17. A.W. Cramb, C. Orrling, Y. Fang, N. Phinichka and S. Sridhar: "Observing and measuring solidification phenomena at high temperatures", *JOM (USA),* 1999, vol. 51 (7), p. 11.

18. P.N. Quested and B.J. Monaghan: "The Measurement of Thermophysical Properties of Molten Slags and Fluxes", *High Temp. Mater. Process,* 2001, vol. 20 (3-4), pp. 219-33.

19. Y. Kashiwaya and K. Ishii: "Fundamental analysis on the heat transfer of the double hot thermocouple for the measurement of thermal diffusivity of molten slag", *Iron & Steel Society International Technology Conference and Exposition 2003*, (Indianapolis, IN, USA, 27-30 Apr. 2003), Iron and Steel Society/AIME, 2003, vol., pp. 1021-32.

20. S. Terada, K. Ryu, S. Kaneko and T. Mitsumune: "Development of a new type of viscometer and estimation of viscosity and solidifying point by calculation formula", *Steelmaking Conference*, (Chicago, IL, USA, 20-23 Mar. 1994), Iron and Steel Society/AIME (USA), 1994, vol. 77, pp. 457-59.

21. B. Mairy, D. Ramelot and M. Dutrieux: "Mold Lubrication and Oscillation Monitoring for Optimizing Continuous Casting", *5th Process Technology Conference: Measurement and Control Instrumentation in the Iron and Steel Industry*, (Detroit, Michigan, USA, 14-17 Apr. 1985), ISS/AIME, Warrendale, PA, 1985, vol., pp. 101-17.

22. J.L. Brendzy, I.A. Bakshi, I.V. Samarasekera and J.K. Brimacombe: "Mould--Strand Interaction in CC of Steel Billets. II. Lubrication and Oscillation Mark Formation", *Ironmaking and Steelmaking (UK),* 1993, vol. 20 (1), pp. 63-74.

23. P. Schergen, M. Houbart and R. Heard: "Vibromold, a flexible tool for succcessful high speed casting of sensitive steel grades", *3rd International Metallurgical Conference on CC of Billets*, (Trinec, Czech Republic, 26-27 Oct. 1999), Trinecke Zelezarny, Trinec, 739 70, Czech Republic, 1999, vol., pp. 67-77.

24. W.H. Emling and S. Dawson: "Mold Instrumentation for Breakout Detection and Control", *74th Steelmaking Conference*, (Washington, D.C., USA, 14-17, Apr. 1991), ISS, Warrendale, PA, 1991, vol. 74, pp. 197-217.

25. P.V. Riboud and M. Larrecq: "Lubrication and Heat Transfer in a Continuous Casting Mold", *Steelmaking Proceedings*, (Detroit, Mich., USA, TMS/AIME, 1979, vol. 62, pp. 78-92.

26. K. Koyama, Y. Nagano, K. Nagano and T. Nakano: "Design for Chemical and Physical Properties of Continuous Casting Powders", *Nippon Steel Tech. Rep.,* 1987, vol. 34, pp. 41-47.

27. I.R. Lee, J.W. Kim, J. Choi, O.D. Kwon and Y.K. Shin: "Development of mould powder for high speed continuous casting", *Conference on Continuous Casting of Steel in Developing Countries*, (Beijing, China, 14-18 Sept. 1993), Chinese Society of Metals, 1993, vol., pp. 814-22.

28. Y. Kashiwaya, C.E. Cicutti and A.W. Cramb: "An investigation of the crystallization of a continuous casting mold slag using the single hot thermocouple technique", *ISIJ International (Japan),* 1998, vol. 38 (4), pp. 357-65.

29. C. Orrling, A.W. Cramb, A. Tilliander and Y. Kashiwaya: "Observations of the melting and solidification behavior of mold slags", *Iron and Steelmaker (USA),* 2000, vol. 27 (1), pp. 53-63.

30. C. Orrling, S. Sridhar and A.W. Cramb: "In situ observation of the role of alumina particles on the crystallization behavior of slags", *ISIJ International (Japan),* 2000, vol. 40 (9), pp. 877-85.

31. K. Watanabe, M. Suzuki, K. Murakami, H. Kondo, A. Miyamoto and T. Shiomi: "The effect of mold powder crystallization on heat transfer in continuous casting mold", *NKK Technical Review (Japan),* 1997, vol. 77, pp. 20-26.

32. M.S. Bhamra, M.G. Charlesworth, S. Wong, D. Sawyers-Villers and A.W. Cramb: "Crystallization of fluxes under varying cooling rates", *54th Electric Furnace Conference*, (Dallas, Texas, USA, 9-12 Dec. 1996), ISS/AIME, Warrendale, PA, 1996, vol. 54, pp. 551-64.

33. S. Seetharaman: "Chapter 2: Pertinent Properties for Metals and Slags in Continuous Casting", in *The Making, Shaping and Treationg of Steel 11th Ed.*, vol. Casting, A. Cramb, ed., AISE Steel Foundation, 2003,

34. K. Tsutsumi, J.I. Ohtake, T. Nagasaka and M. Hino: "Crystallization Behavior of Li2O-SiO2, NA2O-SiO2 and Na2O-CaO-SiO2 Galsses", *Tetsu-to-Hagane (J. Iron Steel Inst. Jpn.),* 1998, vol. 84 (6), pp. 464-69.

35. A. Prasad and H. Henein: "CCT Diagram for Mold Flux Crystallization Studies", *ISSTech 2003*, (Indianapolis, IN, April 27~30), 2003, vol., pp. 257-62.

36. M.D. Lanyi and C.J. Rosa: "Casting Fluxes: Physical Properties Affecting Strand Lubrication", *Ironmaking and Steelmaking,* 1982, vol. 9 (1), pp. 25-31.

37. W.L. McCauley and D. Apelian: "Temperature Dependence of the Viscosity of Liquids", *Proceeding of 2nd International Symposium on Metallurgical Slags and Fluxes*, Meallurigical Society of AIME, Warrendale, PA, 1984, vol., pp. 925-47.

38. K.C. Mills and S. Sridhar: "Viscosities of Ironmaking and Steelmaking Slags", *Ironmaking and Steelmaking (UK),* 1999, vol. 26 (4), pp. 262-68.

39. P.V. Riboud, Y. Roux, L.D. Lucas and H. Gaye: "Improvement of Continuous Casting Powders", *Fachberichte Huttenpraxis Metallweiterverarbeitung,* 1981, vol. 19 (8), pp. 859-69.

40. S. Sridhar, K.C. Mills, O.D.C. Afrange, H.P. Lorz and R. Carli: "Break temperatures of mould fluxes and their relevance to continuous casting", *Ironmaking and Steelmaking (UK),* 2000, vol. 27 (3), pp. 238-42.

41. *High Temperature Tribometer*. Pin-on-disk Friction and Wear (Tribology) Measurement to 1000 DegC, Advanced Mechanical Technology, Inc, 176 Waltham Street, Watertown, MA 02472, USA.

42. D.T.K. Lui: *Effect of Oscillation Marks on Heat Transfer in Continuous Casting Molds*, Master Thesis, UIUC, 1995.

43. A. Prasad, H. Henein and C.A. Gandin: "A Study of Microsegregation in Al-Cu alloys Using Impulse Atomization as an RSP", *Light Metals 2002 Métaux Légers,* (Montreal, Quebec, Canada, 11-14 Aug. 2002), 2002, vol., pp. 101-14.

44. H.E. Sliney and C. Dellacorte: "Friction and wear of ceramic/ceramic and ceramic/metal combinations in sliding contact", *Lubrication Engineering, 19*94, vol. 50 (7), pp. 571-76.

45. R.H. Doremus: Gl*ass Science,* John Wiley & Sons, Inc., New York, 1994.

46. P. Grieveson, S. Bagha, N. Machingawuta, K. Liddell and K.C. Mills: "Physical Properties of Casting Powders. II. Mineralogical Constitution of Slags Formed by Powders", *Ironmaking Steelmaking, 19*88, vol. 15 (4), pp. 181-86.

47. R.J. O'malley: "Glass Film Isothermal Aging Study", *private communication, 20*03.

48. Y. Meng: Mo*deling Interfacial Slag Layer Phenomena In The Shell/Mold Gap In Continuous Casting Of Steel,* PHD Thesis, University of Illinois, Champaign-Urbana, 2004.

49. C. Orrling, S. Sridhar, Y. Kashiwaya and A.W. Cramb: "Crystallization phenomenon in slags", 58*th Electric Furnace Conference and 17th Process Technology Conference,* (Orlando, FL, USA, 12-15 Nov. 2000), ISS/AIME, Warrendale, PA, 2000, vol., pp. 211-21.

Table I Actual Mold Powder Compositions

	S1	S2	K1	H1
SiO_2	34.33	38.33	31.68	36.01
CaO	29.69	13.30	21.52	35.74
Al_2O_3	5.55	2.43	4.85	4.63
CaF_2	15.93	14.05	28.12	6.82
Na_2O	4.75	13.44	9.57	6.04
MgO	3.05	1.45	0.84	<3.0
TiO_2	<1.0	<0.5	-	<3.0
Fe_2O_3	<1.5	<1.5	0.20	<3.0
MnO	<1.0	<0.5	0.01	<3.0
K_2O	<1.0	<0.5	0.80	<3.0
Li_2O	-	<1.0	-	-
B_2O_3	-	1.41	-	-
C-Total	4.11	11.49	2.36	5.73
CO_2 *	3.22	3.78	2.75	-
C-Free *	3.23	10.46	1.61	

*: not counted in percentage calculation

Table II Mold Powder Composition Reported by Suppliers (wt%)

	S1	S2	K1	H1
SiO_2	33.3	37.39	29.93	35.8
CaO	39.9	22.82	39.41	40.4
Al_2O_3	5.38	2.37	4.58	4.6
F	7.52	6.67	12.93	3.3
Na_2O	4.61	13.11	9.04	6.0
MgO	2.96	1.41	0.79	<3.0
TiO_2	<1.0	<0.5	-	<3.0
Fe_2O_3	<1.5	<1.5	0.19	<3.0
MnO	<1.0	<0.5	0.01	<3.0
K_2O	<1.0	<0.5	0.80	<3.0
Li_2O	-	<1.0	-	-
B_2O_3	-	1.38	-	-
C-Total	3.99	11.21	2.23	5.7
CO_2	3.12	3.68	2.62	-
C-Free	3.14	10.21	1.52	-
H_2O @ 105^oC	<0.50	<0.50	-	-
H_2O @ 600^oC	<1.0	<1.0	-	-

Table III Phases Present in Slag S1 after Devitrification Tests

Phases \ Test	700°C 1min	700°C 30min	700°C 60min	900°C 1min	900°C 120min	1100°C 1min	1100°C 60min
Glass	X	X					
Cuspidine ($3CaO•2SiO_2•CaF_2$)		X	X	X	X	X	X
Calcium silicon oxide fluoride ($SiO_2•2CaF_2$)				X	X	X	X
Nepheline ($Na_2O•Al_2O_3•2SiO_2$)				X	X	X	
Gehlenite ($2CaO•2Al_2O_3•SiO_2$)							X

Table IV Phases Present in Slag S2 after Devitrification Tests

Phases \ Test	500°C 120min	700°C 1min	700°C 30min	700°C 120min	900°C 1min	900°C 60min	1000°C 10min
Glass	X	X	X				X
Cuspidine ($3CaO•2SiO_2•CaF_2$)			X	X	X	X	X
Calcium silicate ($2CaO•SiO_2$)			X	X	X	X	
Nepheline ($Na_2O•Al_2O_3•2SiO_2$)				X			
Calcium silicate ($8CaO•5SiO_2$)				X	X		
Sodium calcium silicate ($Na_2O•2CaO•3SiO_2$)						X	

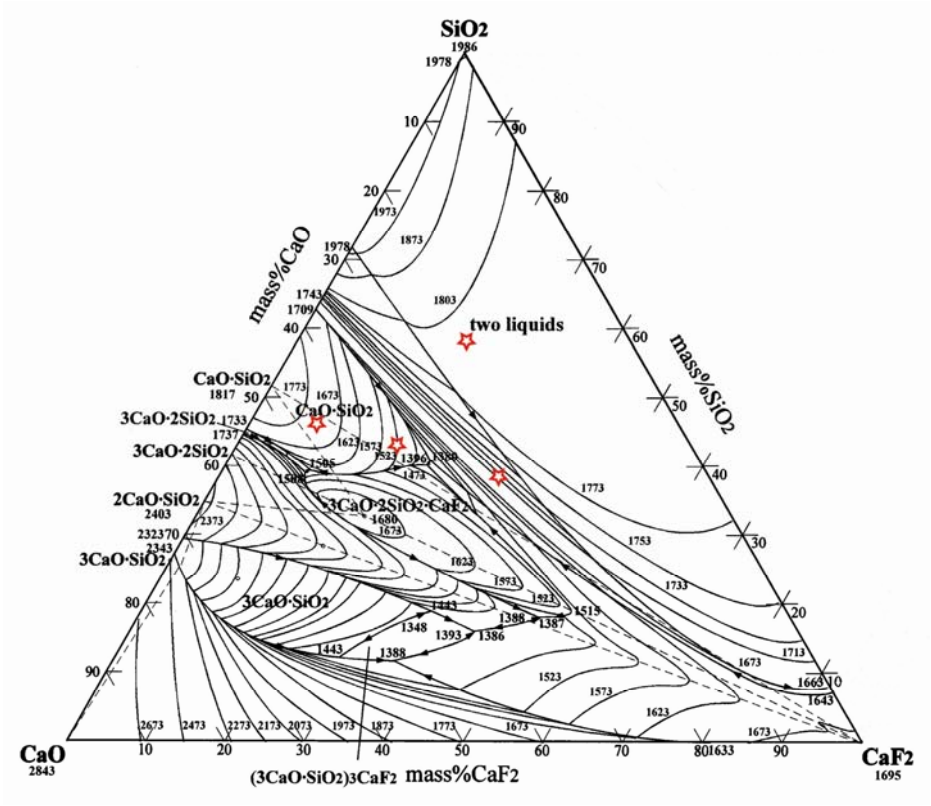

Figure 1: Ternary phase diagram showing liquidus temperature contours

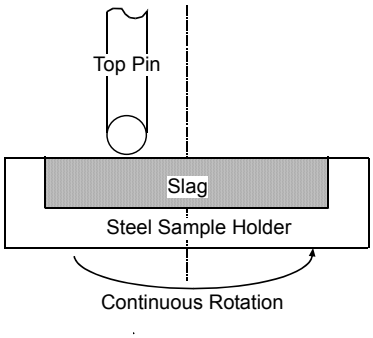


slag S1


slag S2

(a) High Temperature Tribometer

(b) Test Setup

(c) Samples

Figure 2: High Temperature Tribometer

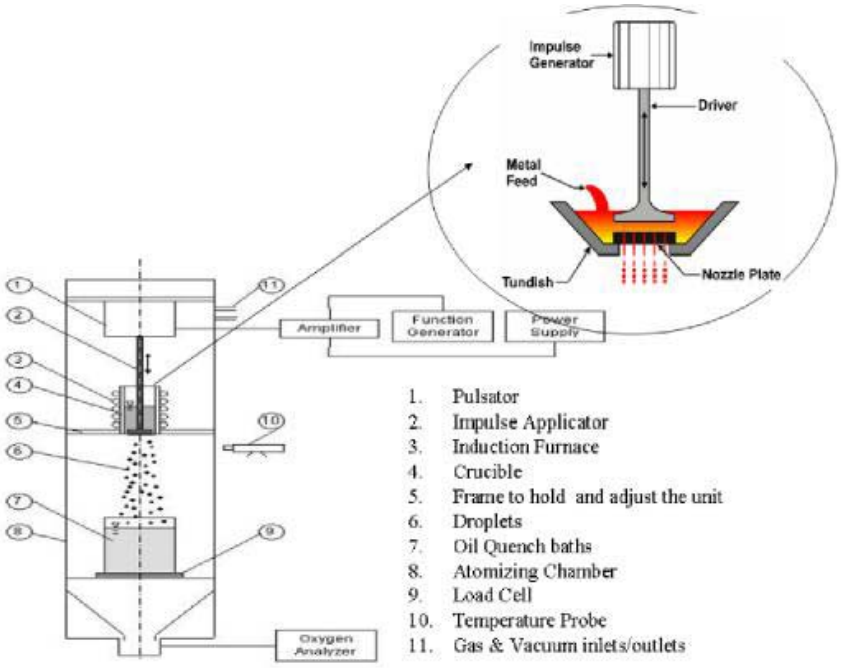

Figure 3 Impulse Atomization Process

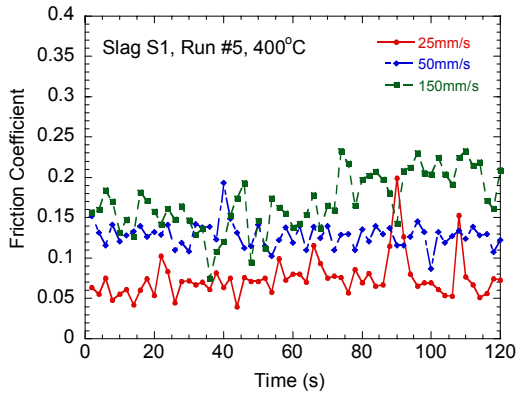

(a) Friction variation with time

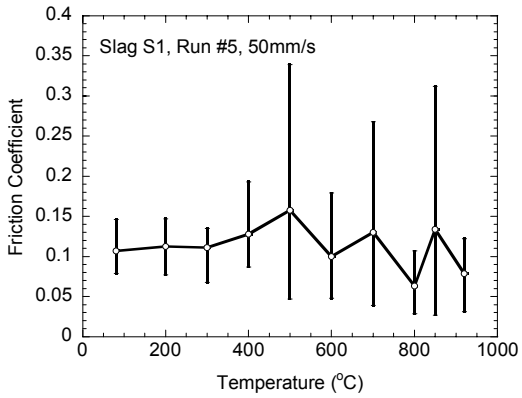

(b) Friction variation with temperature including "error bars" to indicate data ranges

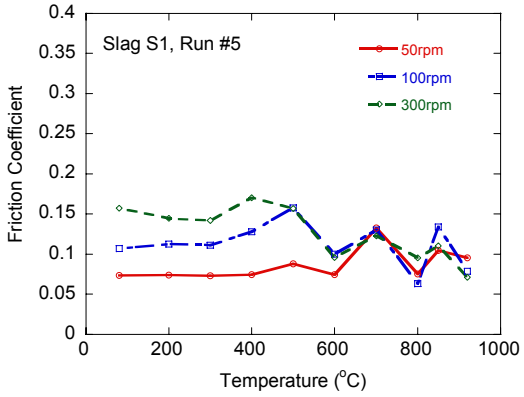

(c) Average friction coefficient vs. temperature at different speeds

Figure 4: Friction coefficient for slag S1 Run #5

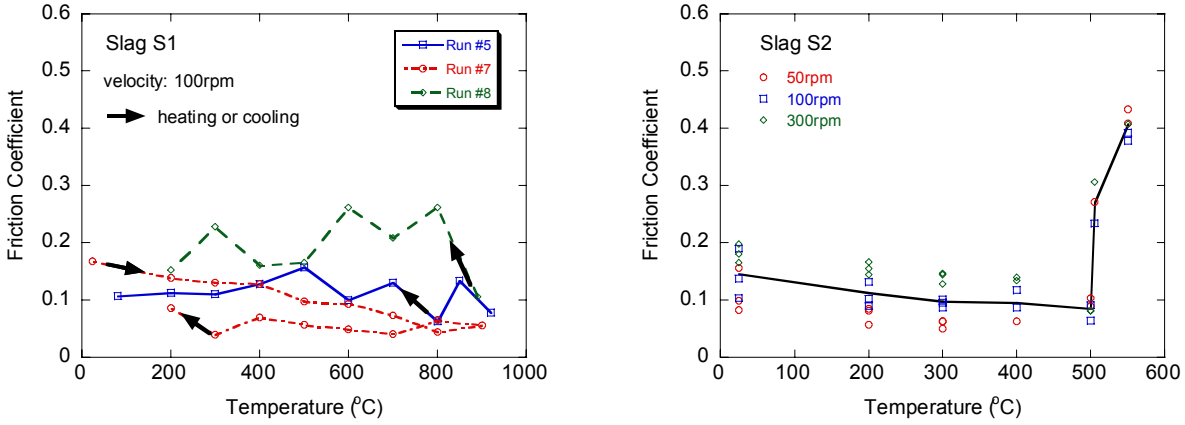

(a) Slag S1 (b) Slag S2

Figure 5: Friction coefficient vs. temperature measured with Tribometer

(a) Slag S1 after Run #5 (b) Slag S2 after Run #6

Figure 6: Slag samples after friction tests

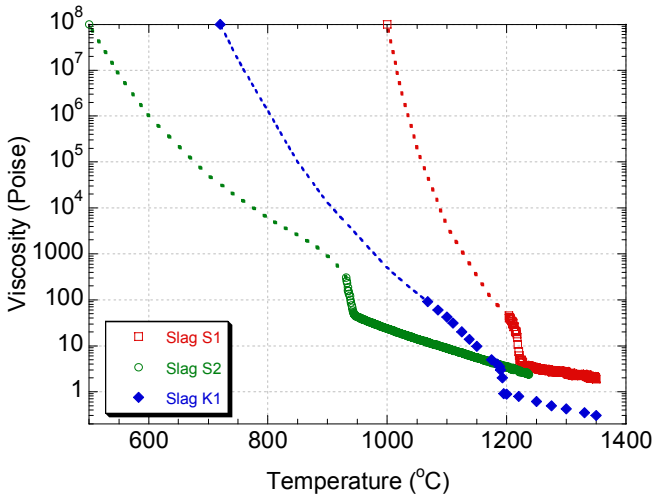

Figure 7: Interpolated viscosity curve

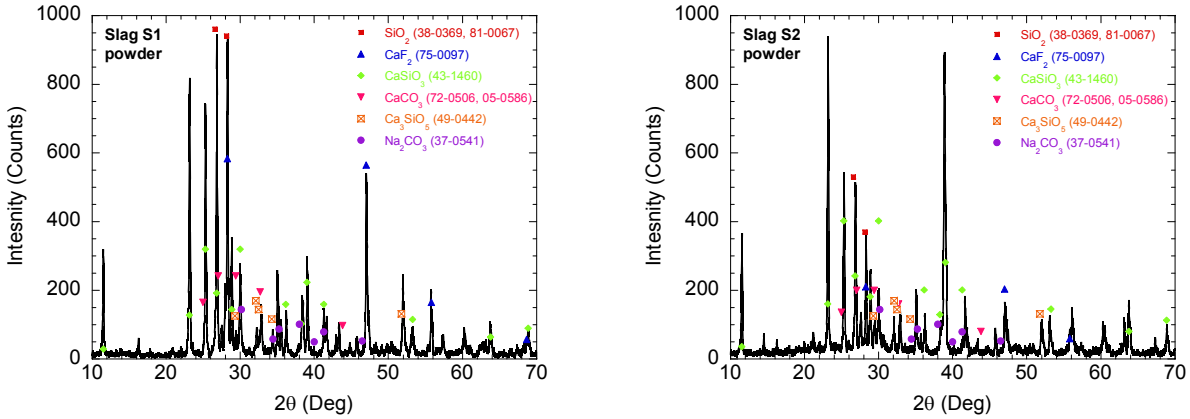

(a) Slag S1 (b) Slag S2

Figure 8: XRD pattern of mold powder

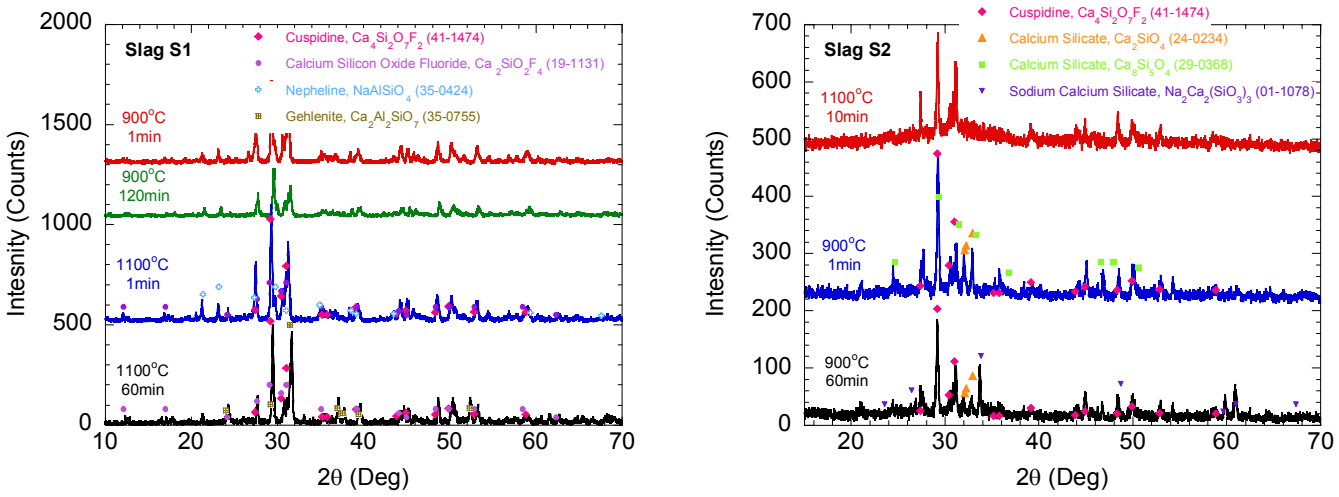

(a) Slag S1 (b) Slag S2

Figure 9: XRD pattern of slag devitrification tests

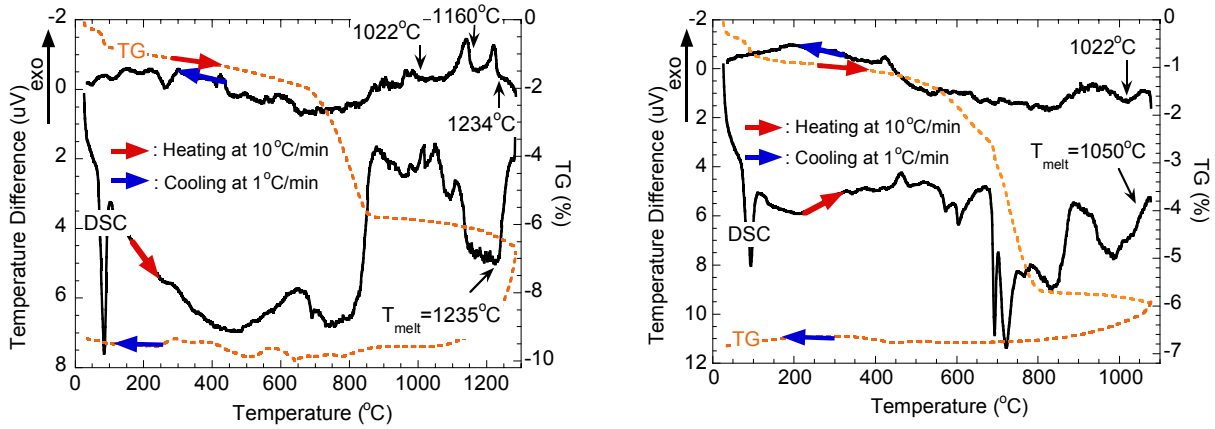

(a) Slag S1 (b) Slag S2

Figure 10: DSC/TG curves at 10°C heating rate and 1°C/min cooling rate

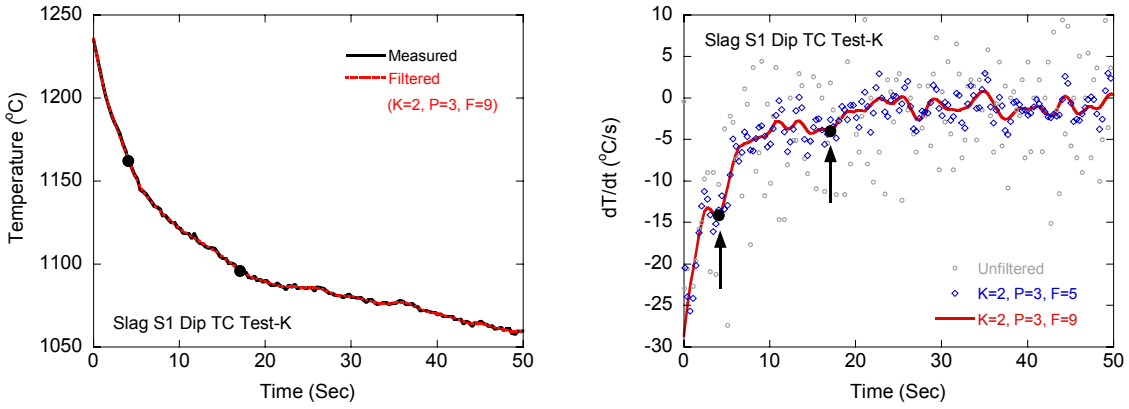

(a) Temperature History of Test K (b) Temperature derivative of Test K

Figure 11: Analysis of TC cooling curves in dip tests

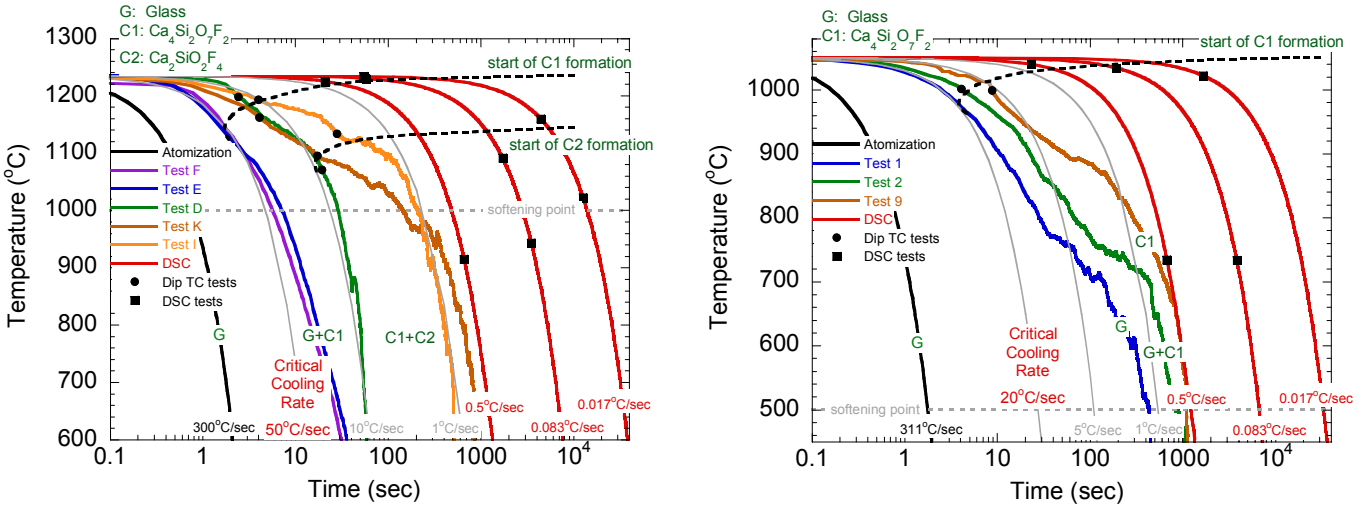

(a) Slag S1 (b) Slag S2

Figure 12: CCT diagrams

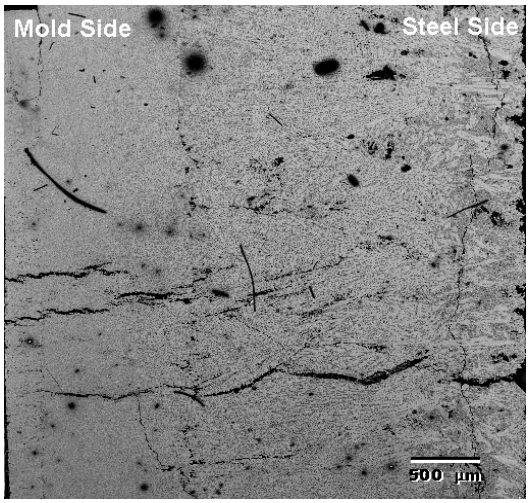

(a) Slag K1

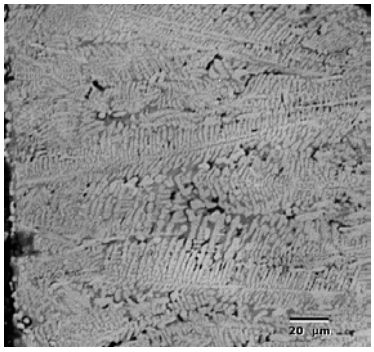

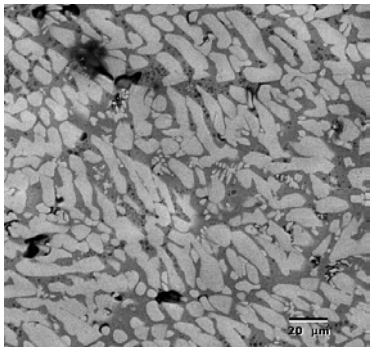

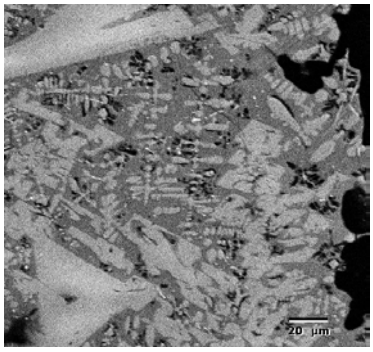

(b) Mold Side (c) Middle Layer (d) Steel Side

Figure 13: BSE images of slag K1 from experimental film

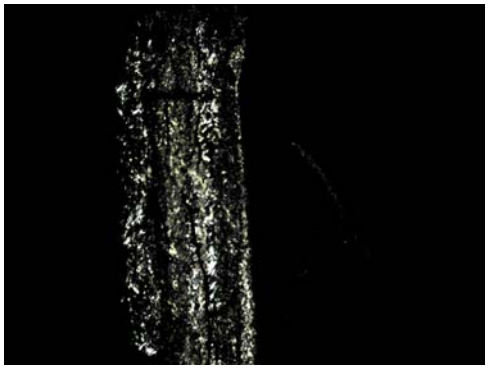

(a) Plane polarized light (b) Cross Polarized light

Figure 14: Polarized light microscopy (slag H1)

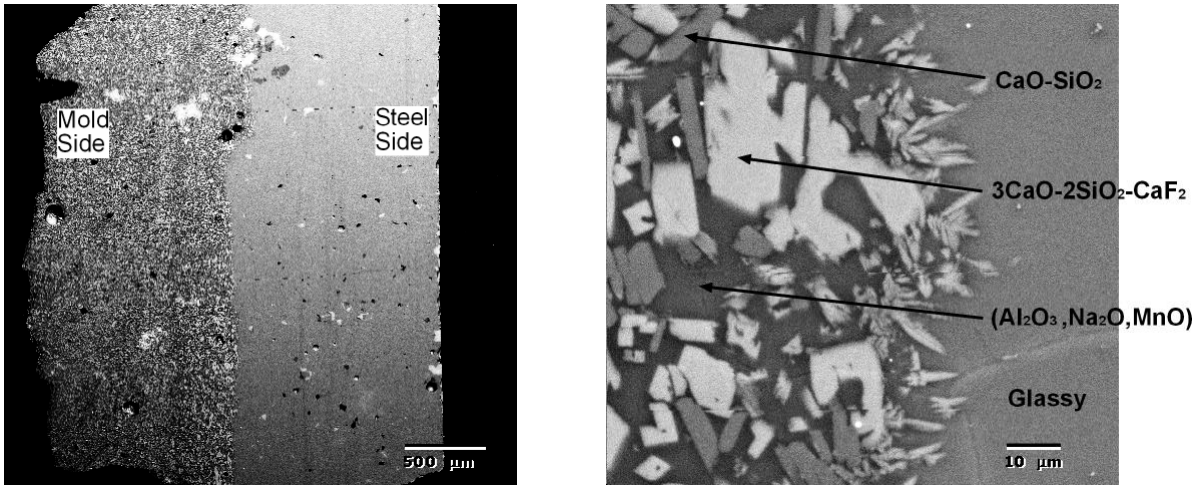

(a) 30X (b) 500X

Figure 15: BSE image of slag H1 film

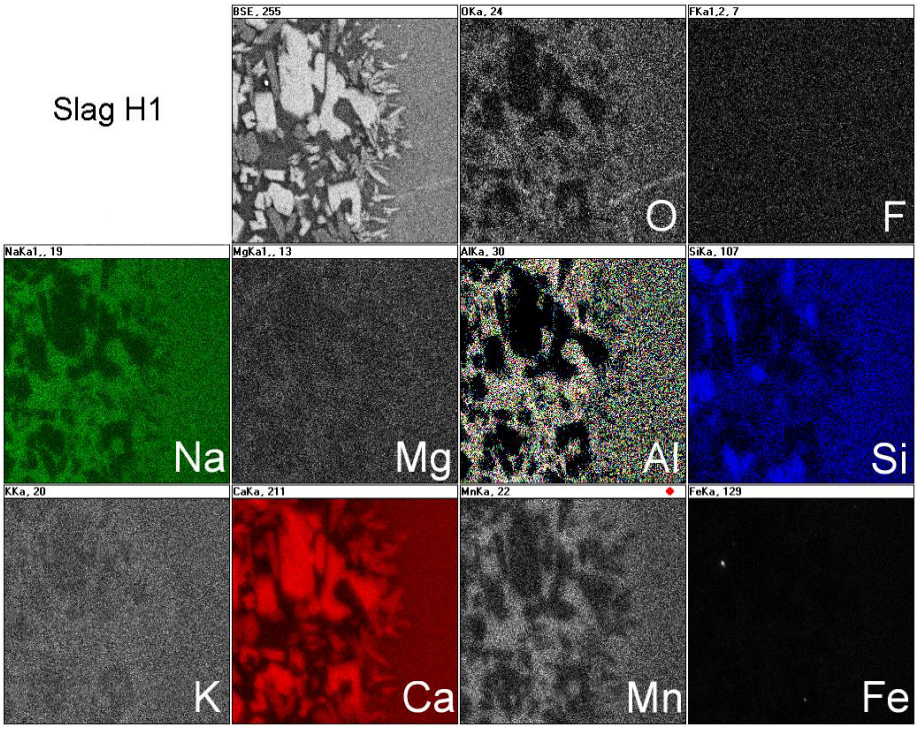

Figure 16: EDX mapping of slag H1 film